Michigan State University

National Superconducting Cyclotron Laboratory

NONSTATISTICAL POPULATIONS OF PARTICLE-UNBOUND STATES IN ^{10}B

C. SCHWARZ, W.G. GONG, N. CARLIN, C.K. GELBKE, Y.D. KIM, W.G. LYNCH, T. MURAKAMI, G. POGGI, R.T. de SOUZA, M.B. TSANG, H.M. XU, K. KWIATKOWSKI, V.E. VIOLA, and S. YENNELLO

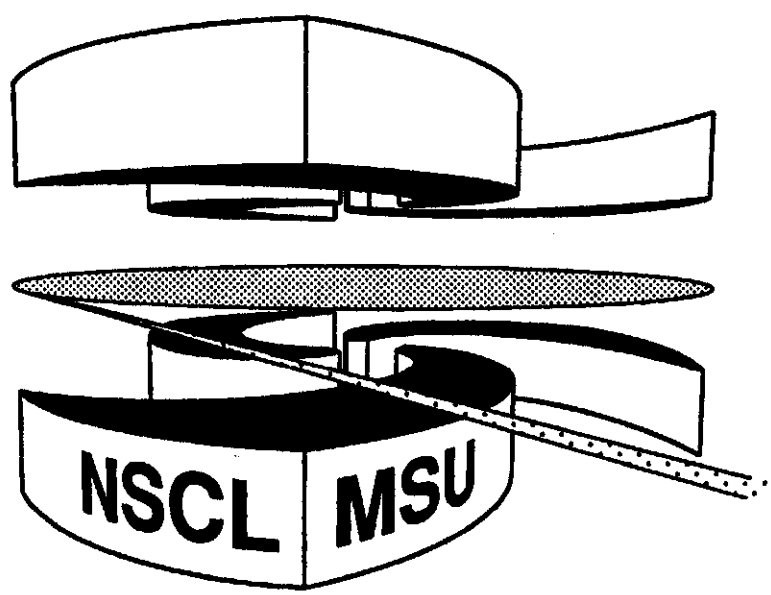

MSUCL-919

JANUARY 1994

Nonstatistical Populations of Particle-Unbound States in ^{10}B

C. Schwarz, W.G. Gong[a], N. Carlinb, C.K. Gelbke, Y.D. Kim[c], W.G. Lynch, T. Murakami[d], G. Poggie, R.T. de Souzaf, M.B. Tsang, and H.M. Xu[g]

National Superconducting Cyclotron Laboratory and Department of Physics and Astronomy, Michigan State University, East Lansing, Michigan 48824, USA

K. Kwiatkowski, V.E. Viola, and S. Yennello[g]

Department of Chemistry and Indiana University Cyclotron Facility, Indiana University, Bloomington, *Indiana 47405*, USA

Abstract:

Relative populations of particle unstable states in ^{10}B were measured for the normal kinematics reactions $^{14}N + ^{27}Al$ and $^{14}N + ^{197}Au$ at E/A =75 MeV, the nearly symmetric reaction $^{129}Xe + ^{122}Sn$ at E/A = 31 MeV, and the inverse kinematics reaction $^{129}Xe + ^{27}Al$ at E/A = 31 MeV. In all cases, the relative populations are incompatible with statistical distributions. For the ^{129}Xe-induced reactions, equilibration appears more complete than for the ^{14}N-induced reactions.

PACS number(s): 25.70.Mn, 25.70.Gh

Highly excited nuclear matter can be formed in intermediate-energy nucleus-nucleus collisions, but the degree of equilibration reached in such collisions is still uncertain. In normal kinematics at forward angles, slopes of inclusive energy spectra show "kinetic" temperatures which are considerably larger than the "emission" temperatures derived from the relative population of states [1-5]. Such differences can be attributed to the effects of cooling and understood within the framework of the expanding compound nucleus model of ref. [6] or on the basis of transport theories [4,7,8]. Differences between kinetic and emission temperatures could also result from a mixing of preequilibrium and evaporative processes, and they have been interpreted in terms of different reaction scenarios [9,10]. Admixtures from nonequilibrium processes could also give rise to nonstatistical populations of states as, for example, observed for emitted ^{10}B fragments [11-13]. To address the question of whether the nonstatistical populations of ^{10}B states are a function of the reaction considered, we analyzed populations of states in ^{10}B for projectile-target combinations in normal and inverse kinematics, and for nearly symmetric collisions using data from a previous experiment [14,15].

The experiment [14] was performed with ^{14}N and ^{129}Xe beams of E/A = 75 and 31 MeV, respectively, extracted from the K1200 cyclotron of the NSCL. For the ^{14}N beam we used ^{27}Al (15 mg/cm^2) and ^{197}Au (15.9 mg/cm^2) targets; for the ^{129}Xe beam the targets were ^{27}Al (5.6 mg/cm^2) and ^{122}Sn (5.3 mg/cm^2). Light charged particles were detected with two _E-E detector arrays, consisting of 300 - 400 μm thick silicon _E-detectors and 10 cm long CsI(Tl) or NaI(Tl) E-detectors. One array, consisting of 37 Si-CsI(Tl) telescopes [16], was centered at the polar and azimuthal angles of $\theta = 25°$ and $\phi = 0°$; each of its detectors had a solid angle of $\_\Omega = 0.37$ msr and a nearest neighbor spacing of $\_\theta = 2.6°$. Isotopic identification was obtained for hydrogen to beryllium nuclei. The other array, consisting of 13 Si-NaI(Tl) telescopes, was centered at $\theta = 25°$ and $\phi = 90°$; each of its detectors had a solid angle of $\_\Omega = 0.5$ msr and a nearest neighbor spacing of $\_\theta = 4.4°$. Particles were identified by isotope up to ^{7}Li. Coincident and downscaled singles data were taken simultaneously. All data were corrected for random coincidences. Energy calibrations for individual detectors were obtained by scattering α-particles of 90, 116, and 160 MeV incident energy from a $(CH_2)_n$ target and by detecting elastically scattered α-particles and recoil protons at various laboratory angles. Energy calibrations for heavier particles were obtained from their energy loss in the semiconductor _E-detectors. The accuracy of energy calibrations is within 2% for p, d, t, ^{3}He, and ^{4}He; it is within 6% for lithium and 9% for boron. For more details see ref. [14].

Single-particle inclusive energy spectra for boron nuclei display maxima close to the exit-channel Coulomb barrier and then decrease exponentially at higher energies. Examples of these spectra, detected at $\theta_{lab} = 18°$, 25°, and 33° (the extreme and average angles covered by the CsI-detector array) are shown in Fig. 1. The energy spectra for the ^{14}N-induced reactions contain significant

preequilibrium components, while those for the ^{129}Xe-induced reactions are dominated by near-equilibrium decays of rapidly moving heavy projectile and/or fusion residues.

For the calculation of the two-fragment detection efficiency [1], we interpolated the yields for the ^{14}N induced reactions with a simple three-source parametrization, Eq. 1 of ref. [5]; the yields for the ^{129}Xe-induced reactions were interpolated with a two-source parametrization assuming a smooth distribution of Coulomb barriers, Eq. 2 of ref. [5]. The quality of these interpolations is shown by the solid curves in Fig. 1. Most detectors did not allow a clean separation of boron isotopes, but a number of telescopes had sufficient _E-resolution to allow determination of the relative yields of B and ^{10}B. In our efficiency calculations, we assumed the angular and kinetic energy distributions of particle stable ^{10}B nuclei and particle unstable ^{10}B* parent nuclei to be the same as those for isotopically unresolved boron nuclei.

Two-particle correlation functions for ^{6}Li + α and ^{9}Be + p are presented in Figs. 2 and 3, respectively, for ^{14}N-induced (upper panels) and ^{129}Xe-induced (lower panels) reactions. The correlation functions were constructed by the "singles" technique:

$$1 + R(q) = C\frac{Y_2(q)}{Y_1(\mathbf{p}_1)Y_1(\mathbf{p}_2)} \quad . \tag{1}$$

Here, Y_1 and Y_2 denote the single- and two-particle inclusive yields, $\mathbf{p}_1$ and $\mathbf{p}_2$ are the measured momenta of particles 1 and 2, q is the momentum of relative motion, and C is a normalization constant chosen such that R(q) $\varnothing$ 0 for large values of q. The correlation functions show clear peaks due to single states or groups of states resulting from the decays ^{10}B* $\varnothing$ ^{6}Li + α and ^{9}Be + p. The locations and spins of the relevant states (see Ref. [12] and references therein) are indicated in the panels for the ^{129}Xe + ^{122}Sn reaction.

In order to extract the populations of particle-unstable states in ^{10}B, the coincidence yield was assumed to be given by $Y_2(q) = Y_c(q) + Y_{back}(q)$, where $Y_c(q)$ denotes the yield from decays of particle unstable ^{10}B nuclei and $Y_{back}(q)$ denotes the background yield resulting from coincident emissions of particles 1 and 2 which are not attributed to decays of ^{10}B* nuclei. The background yield is conveniently expressed [1] in terms of the background correlation function

$$Y_{back}(q) = [1 + R_{back}(q)]Y_1 \quad . \tag{2}$$

In our analysis, we extracted the coincidence yield for the two extreme assumptions about the background correlation function indicated by the dashed curves in Figs. 2 and 3.

The decay coincidence yield is related to the decay excitation energy spectrum, $\left|dn(E^*)/dE^*\right|_c$, of particle unstable ^{10}B nuclei via the relation

$$Y_c(q) = \int dE^* \left\{ \varepsilon(E^*,q) \left| \frac{dn(E^*)}{dE^*} \right|_c \right\} , \tag{3}$$

where the efficiency function, $\varepsilon(E^*, q)$, denotes the probability to detect a particle pair with relative momentum q resulting from the decay into channel c of a particle unstable state of excitation energy E^*. (For a detector of perfect resolution, $E^* = q^2/2M_{red} + Q_c$, where M_{red} and Q_c are the reduced mass and the separation energy for decay into channel c, respectively.) If the line shapes of the decaying states are only weakly influenced by the Coulomb penetrability, as is the case for the states considered here, the decay excitation energy spectrum can be written as

$$\left|\frac{dn(E^*)}{dE^*}\right|_c = \sum_\lambda N_\lambda e^{-E^*/T}(2J_\lambda + 1)\frac{\Gamma_\lambda/2\pi}{(E_\lambda - E^*)^2 + \Gamma_\lambda^2/4}\cdot\frac{\Gamma_{\lambda c}}{\Gamma_\lambda}, \qquad (4)$$

For a thermal distribution, N_λ is independent of the state λ. The states analyzed here are narrow, and the Boltzmann factor varies only little over the resonance width. We therefore write the decay yield as

$$Y_c(q) = \sum_\lambda n_\lambda (2J_\lambda + 1)\frac{\Gamma_{\lambda c}}{\Gamma_\lambda}\int dE^*\left\{e^{(E_\lambda - E^*)/T}\varepsilon(E^*, q)\frac{\Gamma_\lambda/2\pi}{(E_\lambda - E^*)^2 + \Gamma_\lambda^2/4}\right\}, \qquad (5)$$

where we have defined the population probability

$$n_\lambda = N_\lambda e^{-E_\lambda/T}. \qquad (6)$$

By construction, a thermal population of states is characterized by an exponential dependence of the population probability, n_λ, on excitation energy E_λ. We have chosen to normalize the population probability such that $n_\lambda(2J_\lambda + 1)$ is equal to the yield for the state divided by the total yield of the particle stable nucleus. For most states considered here, the exponential term inside the integral of Eq. 5 is inconsequential, but for some of the wider states it introduces a small distortion of the line shape.

In our analysis, we selected a fixed value of T = 2 MeV to describe thermal line shape distortions, and we treated n_λ as an adjustable parameter for each group of states λ. The solid curves in Figs. 2 and 3 show fitted correlation functions calculated as

$$1 + R(q) = 1 + R_{back}(q) + \frac{Y_c(q)}{Y_1(p_1)Y_1(p_2)}. \qquad (7)$$

Here, $Y_c(q)$ was calculated from Eq. 5, $Y_1(p_1)$ and $Y_1(p_2)$ were taken as the experimental singles yields, and $R_{back}(q)$ was a smooth function lying between the bounds indicated by the dashed curves in Figs. 2 and 3.

The solid points in Fig. 4 show the extracted $^{10}B^*$ population probabilities, n_λ, as a function of E_λ. The errors are mostly due to uncertainties of the background subtraction; uncertainties due to different choices of T (in Eq. 5) are small in comparison. The data points for E_λ = 4.8, 5.2, and 6.0 MeV excitation energy were extracted from the α-^{6}Li correlation functions (Fig. 2), and the data points at 7.5 MeV excitation energy from the p-^{9}Be correlation functions (Fig. 3). Exponential population probabilities representing normalized Boltzmann

distributions (taking particle stable states into account) are plotted as dashed lines with the temperatures indicated in Fig. 4.

For all projectile-target combinations, the population probabilities are inconsistent with thermal distributions, the group of states at E_λ = 6.0 MeV being more strongly populated than the lower lying group at E_λ = 5.2 MeV. This observation corroborates previous findings [11-13] of the anomalous role played by the group of states at E_λ = 6.0 MeV. The distributions for ^{129}Xe-induced reactions reflect a higher degree of equilibration than the distributions for ^{14}N-induced reactions (for which preequilibrium contributions are large at forward angles). Evidence for enhanced equilibration in central, as compared to peripheral ^{36}Ar + ^{197}Au collisions at E/A = 35 MeV had been reported in ref. [13]. It is hence conceivable, that even higher degrees of equilibration could be attained when near-central collisions are selected for the Xe-induced reactions. Experimental corroboration (or disproof) of this assumption would be important as it could provide important clues with regard to the applicability of statistical concepts in heavy-ion-induced fragmentation reactions.

Some deviation from a purely exponential dependence of the population probability can be attributed to sequential feeding from higher lying particle-unbound states. Previous investigations [11-13] have shown, however, that these perturbations cannot explain the inverted population of states around E_λ _ 6 MeV. The persistently enhanced population of the group of states at E_λ _ 6 MeV for very different reactions suggests that this anomaly may be of a more general origin and independent of details of the reaction dynamics. For example, it is conceivable that the levels in ^{10}B are populated at a stage of the reaction where perturbations by the surrounding hot nuclear matter affect the ordering of levels which evolve into the asymptotic states. Unfortunately such perturbations cannot yet be computed. It is also conceivable that feeding of the group at E_λ _ 6 MeV could be goverened by branching ratios that differ significantly from those assumed in the Hauser-Feshbach model [12]. Alternatively, the spectroscopic information for ^{10}B may not be complete and there may be an additional unresolved state in the group of levels at E_λ = 6.0 MeV [17]. In fact, calculations by Warburton et al. [17] predicted a 3^+ state in ^{10}B around an excitation energy of 6 MeV. If such an unresolved state existed and if it were populated according to its statistical weight, it would lead to a decreased population probability for the group at E_λ _ 6.0 MeV. The open points in Fig. 4 show how such a state could modify the extracted value of n_λ. We should caution, however, that the existence of this 3^+ state is highly uncertain since, to our knowledge, it has never been confirmed experimentally.

In conclusion, we extracted relative populations of states of particle unstable ^{10}B nuclei in normal kinematics for ^{14}N-induced reactions for ^{27}Al and ^{197}Au targets and compared them to those measured for the inverse kinematics ^{129}Xe + ^{27}Al reaction and the nearly symmetric ^{129}Xe + ^{122}Sn reaction. The highest degree of equilibration was observed for the ^{129}Xe + ^{122}Sn reaction. In all

systems we found a nonthermal population probability for the group of states at 6.0 MeV excitation energy. For the reactions measured in normal kinematics, preequilibrium emission could be invoked to account for the observed nonthermal populations of states, but it is surprising to find such anomalies for the ^{129}Xe-induced reactions for which equilibrium emission should predominate.

This work was supported by the National Science Foundation under Grant No. PHY-89-13815 and the Department of Energy under Grant No. DE.FG-0288ER.40404.A. W.G.L. acknowledges the receipt of U.S. Presidential Young Investigator award, N.C. acknowledges partial support by the FAPESP, Brazil, and C.S. acknowledges partial support by the Deutsche Forschungsgesellschaft, Germany.

References

[a] Present address: Nuclear Science Division, Lawrence Berkeley Laboratory, Berkeley, CA 94720, USA

[b] Present address: Instituto de Fisica, Universidade de São Paulo, C. Postal 20516, CEP 01498, São Paulo, Brazil.

[c] Present address: National Lab. for High Energy Physics (KEK),Department of Physics, 1-1 Oho, Tsukuba, Ibaraki 305, Japan.

[d] Present address: Department of Physics, Kyoto University, Kyoto 606, Japan.

[e] Present address: Dipartimento di Fisica dell'Universita and INFN, Largo Enrico Fermi 2, 50125 Firenze, Italy.

[f] Present address: Department of Chemistry, Indiana University Cyclotron Facility, Indiana University, Bloomington, Indiana 47405, USA

[g] Present address: Cyclotron Institute, Texas A&M University, College Station, Texas 77843, USA

1. J. Pochodzalla et al., Phys. Rev. **C35**, 1695 (1987).
2. Z. Chen et al., Phys. Rev. **C36**, 2297 (1987).
3. H.M. Xu et al., Phys. Rev. **C40**, 186 (1989).
4. G.J. Kunde et al., Phys. Lett. **B272**, 202 (1991).
5. C. Schwarz et al., Phys. Rev. **C48**, 676 (1993).
6. W.A. Friedman, Phys. Rev. Lett. 60, 2125 (1988).
7. D.H. Boal et al., Phys. Rev. C40, 601 (1989).
8. H.M. Xu, Phys. Lett. **B299**, 199 (1993).
9. D. Fox et al., Phys. Rev. **C38**, 146 (1988).
10. C. Schwarz et al., Phys. Lett. **B279**, 223 (1992).
11. T.K. Nayak et al., Phys. Rev. Lett. **62**, 1021 (1989).
12. T.K. Nayak et al., Phys. Rev. **C45**, 132 (1992).
13. F. Zhu et al., Phys. Lett. **B282**, 299 (1992).
14. W.G. Gong, PhD Thesis, Michigan State University, 1991.
15. W.G. Gong et al., Phys. Rev. **C43**, 1804 (1991).
16. W.G. Gong et al., Nucl. Instr. and Meth. **A286**, 190 (1988).
17. E.K. Warburton and B.A. Brown, Phys. Rev. **C46**, 923 (1992).

Figure Captions

Fig. 1: Inclusive yields of B fragments detected at θ_{lab}=18°, 25°, and 33°, in reactions of $^{129}Xe + ^{27}Al$ and $^{129}Xe + ^{122}Sn$ at E/A = 31 MeV (bottom panels) and $^{14}N + ^{27}Al$ and $^{14}N + ^{197}Au$ at E/A = 75 MeV (top panels). The solid curves show analytical interpolations of the cross sections used in the calculation of the efficiency function $\varepsilon(E^*, q)$.

Fig. 2: α - ^{6}Li correlation functions measured for the reactions $^{14}N + ^{27}Al$ and $^{14}N + ^{197}Au$ at E/A = 75 MeV (top panels) and $^{129}Xe + ^{27}Al$ and $^{129}Xe + ^{122}Sn$ at E/A = 31 MeV (bottom panels). The fit represented by the solid line is explained in the text. The dashed lines are extreme bounds for the background correlation function. The correlation functions were normalized at q = 160 - 290 MeV/c for the ^{14}N-induced reactions and at q = 200 - 290 MeV/c for the ^{129}Xe induced reactions, respectively.

Fig. 3: p - ^{9}Be correlation functions measured for the reactions $^{14}N + ^{27}Al$ and $^{14}N + ^{197}Au$ at E/A = 75 MeV (top panels) and $^{129}Xe + ^{27}Al$ and $^{129}Xe + ^{122}Sn$ at E/A = 31 MeV (bottom panels). The fit represented by the solid line is explained in the text. The dashed lines are extreme bounds for the background correlation function. The correlation functions were normalized at q = 110 - 160 MeV/c for the ^{14}N-induced reactions and at q = 100 - 160 MeV/c for the ^{129}Xe induced reactions, respectively.

Fig. 4: Population probabilities of particle unstable states in ^{10}B (solid points) extracted for the reactions $^{14}N + ^{27}Al$ and $^{14}N + ^{197}Au$ at E/A = 75 MeV (top panels) and $^{129}Xe + ^{27}Al$ and $^{129}Xe + ^{122}Sn$ at E/A = 31 MeV (bottom panels). Inclusion of an additional 3^+ state in the group at E_λ = 6 MeV gives the lower population probability indicated by the open point. The vertical scale is normalized so that $\sum_k (2J_k + 1)n_k = 1$, where the summation is restricted to the particle stable states of ^{10}B. The dashed lines represent (normalized) Boltzmann distributions of the indicated temperatures.

MSU-94-004

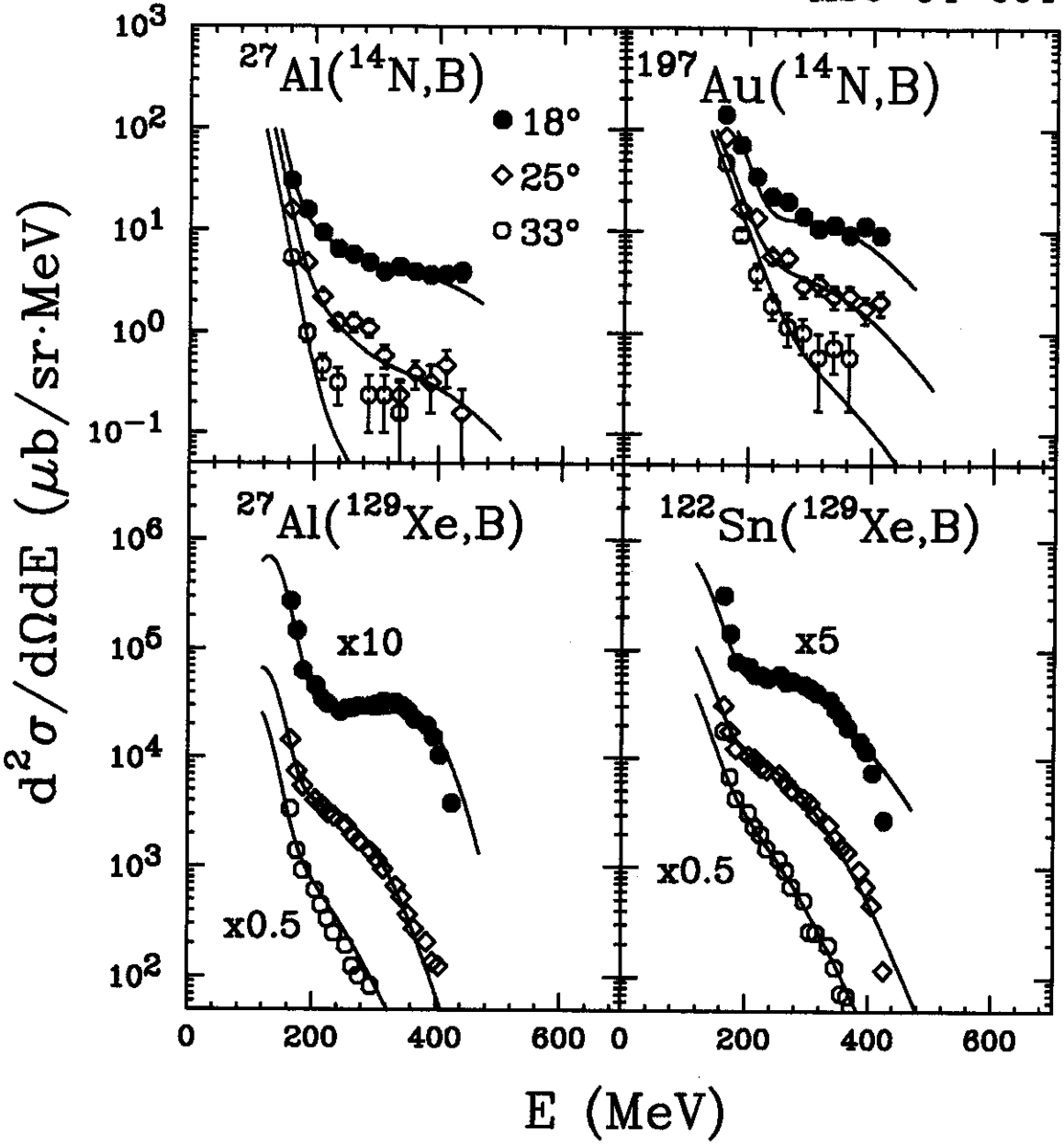

Fig. 1

MSU−94−005

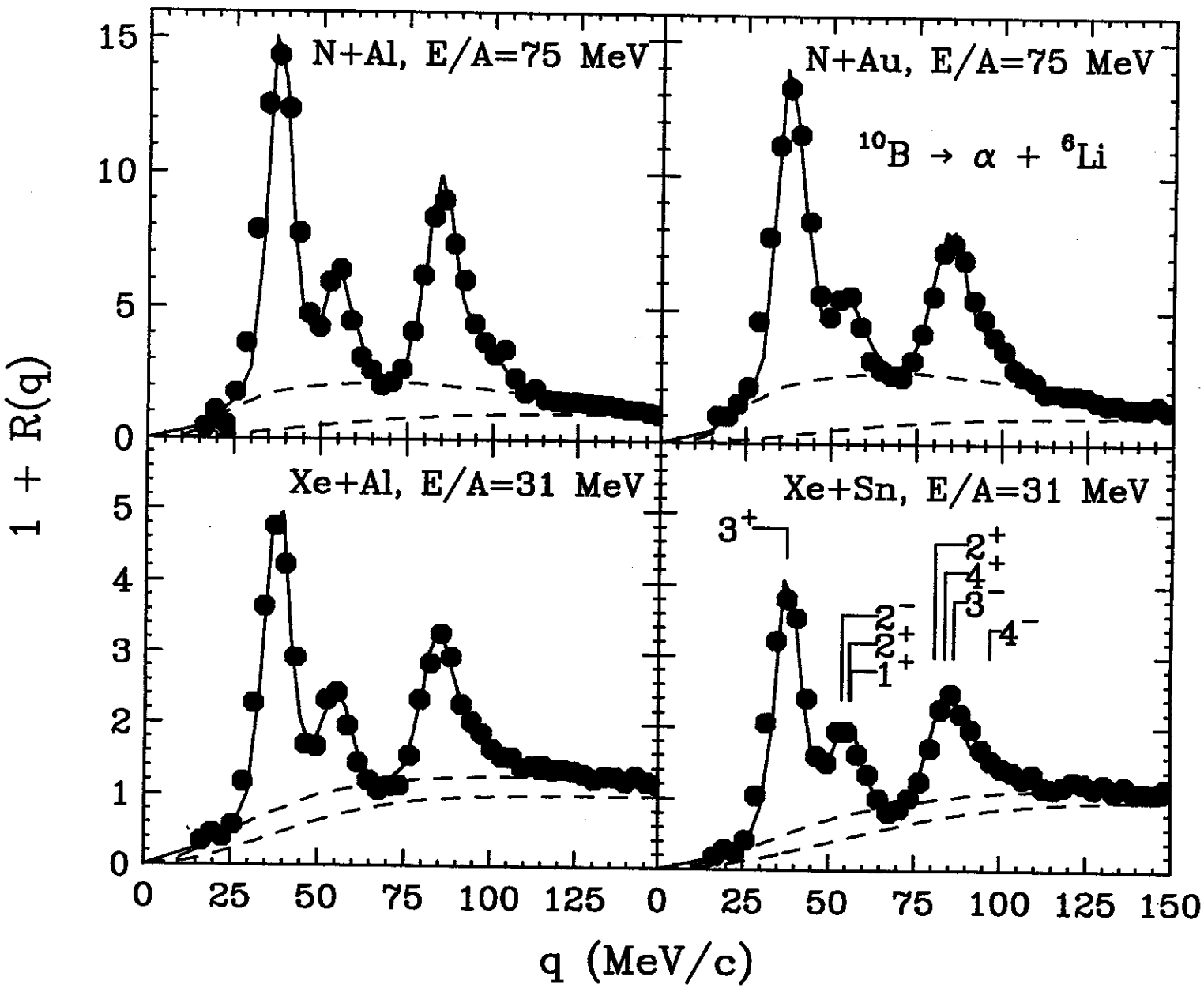
N+Al, E/A=75 MeV
N+Au, E/A=75 MeV
$^{10}B \rightarrow \alpha + {}^{6}Li$
Xe+Al, E/A=31 MeV
Xe+Sn, E/A=31 MeV
3+
2+
4+
3−
2−
2+
1+
4−
1 + R(q)
q (MeV/c)
0
5
10
15
25
50
75
100
125
150

MSU−94−006

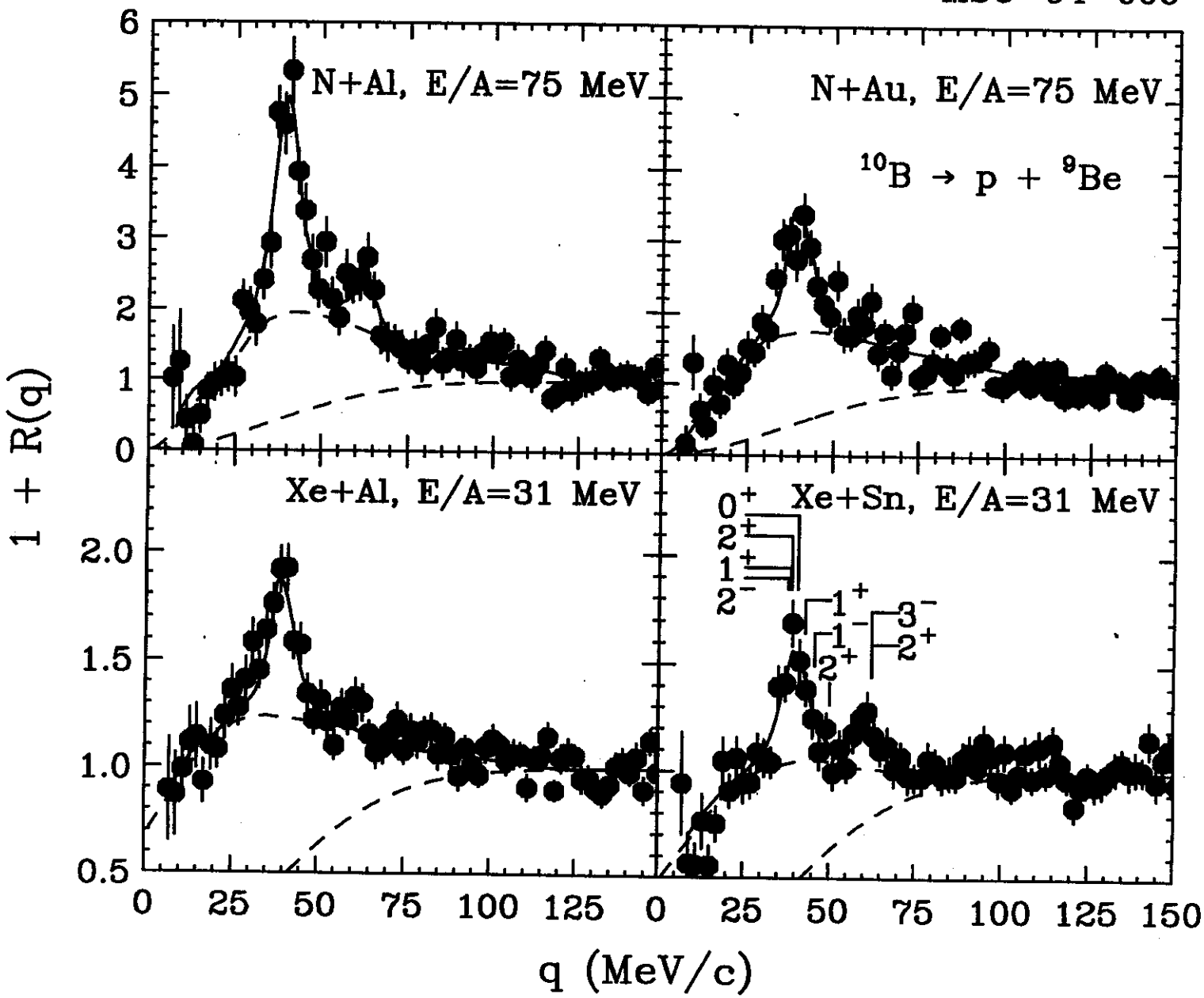

Fig. 3

MSU-94-007

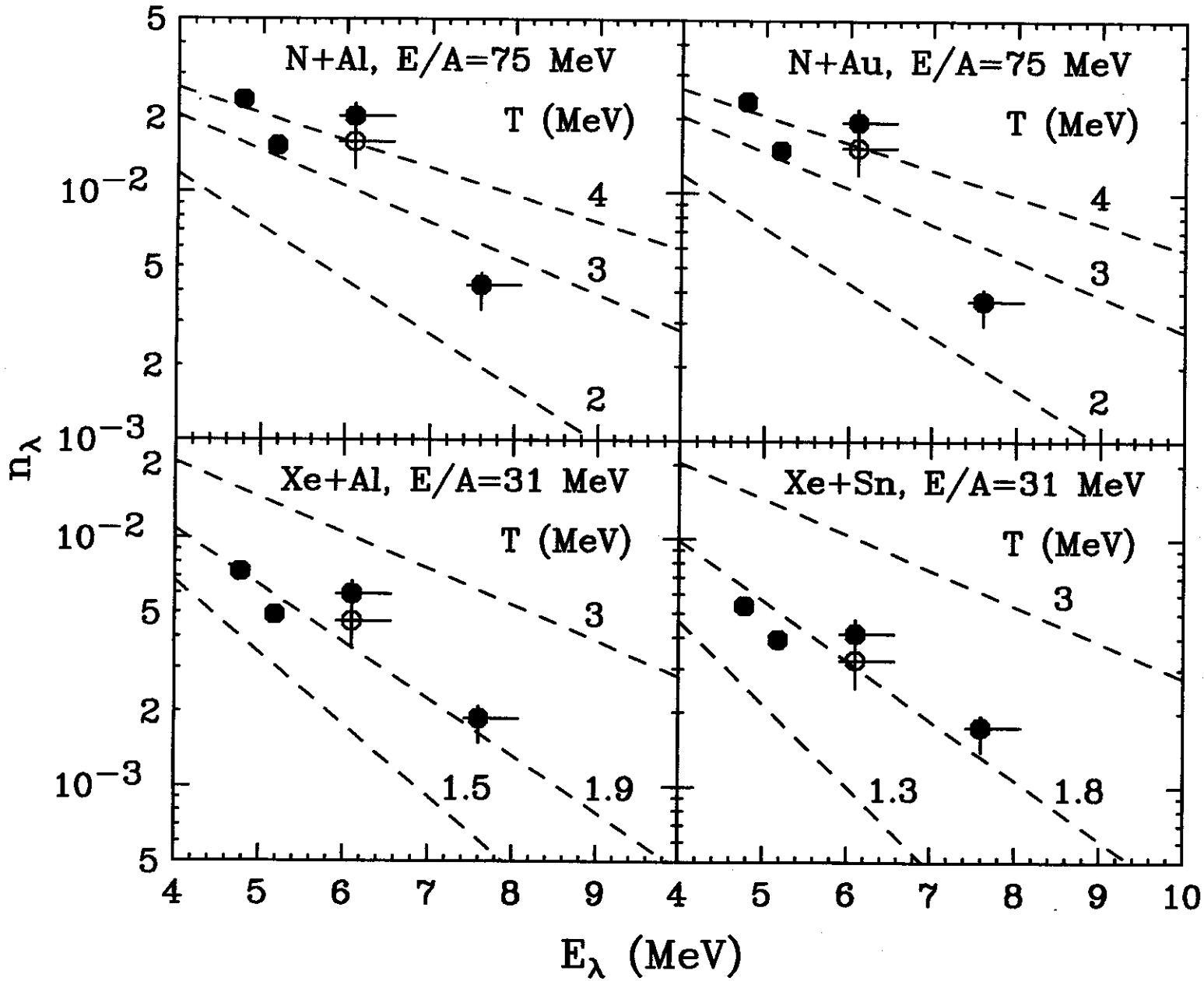

Fig. 4